Layered Perovskite with Compact Morphology and Reduced Grain Size via Vacuum Assisted Crystallization for Light Emitting Diode Application

Article *in* Optical Materials Express · March 2020

DOI: 10.1364/OME.390077

Research Article Vol. 10, No. 5 / 1 May 2020 / Optical Materials Express 1182

Optical Materials EXPRESS

Layered perovskite with compact morphology and reduced grain size via vacuum assisted crystallization for luminescence applications

KHINE ZIN SWE,[1] ATITTAYA NAIKAEW,[1] PAPHADA KAEWURAI,[1] PIMSUDA PANSA-NGAT,[1] SOMBOON SAHASITHIWAT,[2] LAONGDAO KANGKAEW,[2] SUPAGORN RUGMAI,[3] SIRIWAT SOONTARANON,[3] AND PONGSAKORN KANJANABOOS[1,4,*]

[1] *School of Materials Science and Innovation, Faculty of Science, Mahidol University, Bangkok, 10400, Thailand*
[2] *National Metal and Materials Technology Center (MTEC), 114 Thailand Science Park, Phahonyothin Road, Khlong Luang, Pathum Thani, 12120, Thailand*
[3] *Synchrotron Light Research Institute, 111 Moo 6 University Avenue, Muang District, Nakonratchasima, 30000, Thailand*
[4] *Center of Excellence for Innovation in Chemistry (PERCH-CIC), Ministry of Higher Education, Science, Research and Innovation, Bangkok 10400, Thailand*
[*] *Pongsakorn.kan@mahidol.edu*

Abstract: Perovskite materials have gained a lot of interest in LED application because of their excellent properties, such as direct band gap nature, high photoluminescence quantum efficiency (PLQE), high charge carrier mobility, pure color emission with small full width at half maximum, and low non-radiative recombination rate. In this work, we for the first time, developed a new protocol called vacuum assisted crystallization (VAC) for perovskite luminescence applications and optimized different parameters i.e. vacuum pressure, holding time, and annealing time. VAC is an after-deposition process applicable to control nanoscale domain structure and improve phase distribution for various deposition techniques, causing small grain size and dense formation beneficial for high luminescence. Large PLQE enhancement, smooth bright emission, high stability, and good surface morphology were obtained with VAC treatment.

1. Introduction

Organic-inorganic hybrid perovskite materials have been widely used for solar cell application because of their excellent properties such as tunable band gap, low cost, simple solution-processable, high charge carrier mobility, high absorption coefficient, balanced electron hole mobility, and long exciton diffusion length [1–6]. However, perovskite materials are also suitable for other optoelectronic devices such as light emitting diodes, photo detectors, and lasers [4,7, 8]. Unique properties such as high photoluminescence efficiency, direct band gap, narrow emission width, smooth morphology, and high color purity make low-dimension perovskite suitable for luminescence applications and perovskite light emitting diodes (PeLED) [9–12]. Via perovskite inks, thin film deposition methods require low-cost [13–15] and low-energy solution processes i.e. spin coating [13], spray coating [16], dip coating [17], and slot-die printing [18].

There are different crystallization methods for perovskite films. For example, *Sandy et al.* introduced flash infrared annealing (FIRA) crystallization method to get highly stable perovskite solar cells. FIRA helps to achieve bigger grains by collapsing neighborhood grains at the boundary, as additional cations planarize the perovskite film [19]. Post annealed-free (PAF) method is done by diethyl ether immersion to make uniform, large grain with high crystallinity [20].

#390077 https://doi.org/10.1364/OME.390077
Journal © 2020 Received 10 Feb 2020; revised 26 Mar 2020; accepted 27 Mar 2020; published 9 Apr 2020

Optical Materials EXPRESS

Pressure below the saturated vapor greatly accelerates solvent evaporation rate and could increase nucleation sites, reducing grain growth as each site completes over surface area [21,22]. Besides solution processes, vacuum pressure was applied in vapor deposition methods for perovskite solar cell like vapor-assisted solution process [23,24], resulting in desirable structural phases with pinhole-free and smooth surface morphology from over-rapid reaction of perovskite precursors. Brief vacuum exposure (20 s) or vacuum-flash solution process (VASP) after perovskite deposition greatly affects evaporation rate of remaining solvents, causing rapid crystallization and uniform morphology with good interconnectivity and electronic properties suitable for solar cell application [25]. When solar perovskite thin films are formed under vacuum environment for the whole process via vacuum assisted deposition (VAD), the films gain high resistivity to UV, moisture, heat, and mechanical impact, as appropriate vacuum pressure causes gap-free and compact morphology while retaining large grain size for solar application; numerous nucleation sites are forced to grow under limited surface, forming tight packing morphology [23].

According to previous studies [3,4,26–28], smaller perovskite grains are beneficial for luminescence and light emitting diode applications due to reduced diffusion length, enhanced spatial confinement, and therefore larger electron binding energy with small compact grains. Therefore, vacuum treatment has a great potential to achieve both small grain size and compact morphology in one shot. In this work, we for the first time, applied vacuum treatment to layered or low dimension perovskite materials by developing vacuum assisted crystallization (VAC). With VAC, high vacuum pressure was immediately introduced to spin-deposited layered perovskite thin films for a prolonged period of time to rush crystallization, followed by heat treatment in air. Figure 1 shows the VAC process. The freshly-prepared film was treated under predetermined values of pressure and time duration.

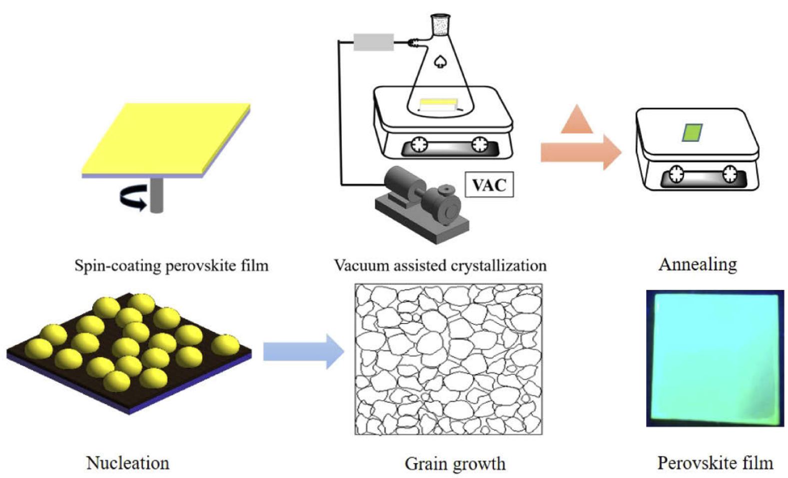

Fig. 1. The process of vacuum assisted crystallization and its mechanism in increasing nucleation sites and reducing grain sizes. The photo shows green luminescence from VAC treatment.

3D inorganic bulk $CsPbBr_3$ perovskite provides unique properties i.e. high color purity, broadly tunable photoluminescence, and high thermal stability, yet 3D perovskite has low electron-hole recombination rate due to low exciton binding energy [6,27]. On the other hand, layered perovskites demonstrate great potential for PeLED application as they possess large exciton binding energy along with wide band gap [4]. The layered perovskite (also known as quasi-2D or 2D Ruddlesden–Popper perovskite) is $L_2A_{n-1}Pb_nX_{3n+1}$, where L is a long aliphatic or aromatic chain such as butyl ammonium (BUA), benzyl ammonium (BA) [28], propyl phenyl ammonium (PPA), and phenylethyl ammonium (PEA) [5]. The assemble of multiple quantum

Optical Materials EXPRESS

wells in layered perovskite structure facilitates the formation of exciton and reduces the possibility of exciton dissociation, leading to increased efficiency of luminescence. However, the mixture of phases and some impurities could cause poor surface morphology and defects, resulting in non-radiative combination [5,13,30,31]. PEABr is an appropriate large organic cation which can reduce dimension of the 3D $CsPbBr_3$ crystal because of stronger hydrogen bond [6] between the hydrogen atom of PEABr and the bromide atoms compared to the bond between Cs^+ and Br^-. In this work, via VAC, we successfully improved PEABr inclusion and reduced nanoscale domain size, hence increasing radiative recombination of the layered perovskite. The VAC thin films feature smaller grain, smoother surface, higher density, higher photoluminescence quantum efficiency, longer average photoluminescence lifetime, and better stability, beneficial for future perovskite light emitting diode application.

2. Experimental

Cesium bromide (CsBr), lead (II) bromide ($PbBr_2$, 98% purity), phenylethylammonium bromide (PEABr), anhydrous dimethyl sulfoxide (DMSO, 99.5% v/v), and 18-crown-6 were purchased from Sigma-Aldrich. Fluorine doped tin-oxide (FTO) were used. The cleaning method of FTO was in the following steps. All the substrates were placed into a tray with alconox soapy water, then sonicated at 60 °C for an hour and rinsed for 3 times. 2-isopropanol was then used under sonication for 30 mins. The substrates were dry with nitrogen blower. The substrates were always treated with UV ozone cleaner before experiment.

CsBr and $PbBr_2$ of 0.2 M were used. PEABr/$CsPbBr_3$ molar ratio = 80% molar, meaning 0.16 M of PEABr was used in this experiment. 3.5 mg/ml of 1,4,7,10,13,16-hexaoxacyclooctadecane or 18-crown-6 was added [6]. All the chemical powders were mixed into dimethyl sulfoxide (DMSO). The solution was stirred on the hotplate at 80 °C for 2 hours to dissolve all chemicals completely, then filtered with polytetrafluorethylene (PTFE, 0.45 μm).

The perovskite precursor solution was dropped onto the substrate and spun under 2 speeds with the spin rate of 1000 r.p.m. for 5 s with 500 r.p.m./s acceleration and 3000 r.p.m. for 55 s with 1500 r.p.m./s acceleration under glovebox environment. The traditional spinning method sample was named as a control. For the control sample, after spin coating, the film was annealed at 100 °C for one min to achieve dry and homogenous morphology. For the VAC sample, after spin coating, the VAC film was immediately kept under a controlled vacuum environment (optimized value of 40 Pa). The setup is consisted of vacuum chamber, pump, pressure controller, and pressure gauge. When the pressure reached the desired value, the time duration was then counted (optimized value of 3 mins). The film was then annealed on a hotplate at 100 °C for 1 min.

Photoluminescence (PL) and photoluminescence quantum efficiency (PLQE) were characterized by photoluminescence spectrometry (Horiba FluoroMax-4P, 150 W xenon lamp excitation source) with Horiba K-Sphere integration sphere (370 nm excitation). Surface morphologies and thickness were studied by field emission scanning electron microscope (FESEM, HITACHI SU8010, 10kv, SE). The absorbance was recorded by UV-Visible spectroscopy (Shimadzu UV-2600). The optical bandgap was obtained by Tauc plot. The crystal structure was studied by X-ray diffractometer (XRD-bench top-Aries from Malvern Panalytical) with scan speed of 0.1402 °/s, 39.525 s of time per step, and the total of 2991 steps. The photoluminescence lifetime (also known as time-resolved photoluminescence) was measured by a Horiba Jobin Yvon FluoroMax-4 spectrofluometer with time correlated single photon counting (TCSPS) unit by using the NanoLED emitting pulses at 370 nm as an excitation source.

3. Results and discussion

Vacuum pressure and time duration followed by annealing time in air were optimized in this work. The perovskite film performance under various pressures can be seen in the Fig. 5. The optimization of time duration under vacuum environment is shown in Fig. 6 and the optimization

Optical Materials EXPRESS

of annealing time variation results is shown in Fig. 7 in the appendix section. Therefore, the optimized parameters of VAC are vacuum pressure of 40 Pa, time duration of 3 mins, and annealing time of 1 min.

The XRD data of the layered perovskite material used in this work is shown in Fig. 2(a). In agreement with previous literature [6], the layered perovskite phases, labelled (⊖), are described at 15.8° and 31.3° which are corresponded to the (100) and (200) planes [6]. As we used the FTO substrate, its XRD peaks are labelled by (*) at 24.5°, 27.1°, 34.4°, and 38.4° [15]. The peaks at 14.5° and 22.3° are the characteristic peaks of $CsPbBr_3$ [32]. The XRD peaks of PEABr labelled by (#) are at 5.2°, 11.6°, and 28.2 [6]. By comparing XRD data of control and VAC, PEABr peaks of VAC sample show lower intensity than the control sample. Because of the vacuum treatment, we could observe that PEABr is better incorporated within perovskite crystals with less PEABr segregation in the film. Pure $CsPbBr_3$ phase is also less pronounced. The better phase distribution from improved PEABr incorporation via VAC is further confirmed by the grazing incidence wide angle X-ray scattering (GIWAXS) experiment shown in Fig. 8 in appendix section. The scattering peak of PEABr shows preferential orientation along the out-of-plane direction at q_z value of 8 nm^{-1}(2-theta = 5.13). According to the literature review, pure PEABr has the peak at 2-theta of 5.13 and 10.27 [6]. From Fig. 8(a-b), the PEABr scattering peak of the control samples are dominant, which can also be observed in XRD patterns. It suggests that the added PEABr is being separated from the perovskite structure. On the other hand, immediately placing the as-casted control sample inside the vacuum chamber is proven to reduce the PEABr phase separation. In Fig. 8(d), we barely observe the PEABr scattering peak from the VAC sample which is treated in vacuum for 3 mins. Low pressure in VAC process helps incorporating the large organic cation (PEA^+) into perovskite structure.

Normalized PL intensities are almost identical for both control and VAC samples as observed in Fig. 2(b). However, the peak of VAC sample is slightly blue-shifted from 510 nm to 490 nm. The blue shift in PL is caused by less trap densities [33,34].

To investigate the material structure on excited states, an optical absorption of the layered perovskite film is shown in Fig. 2(c). A peak near 520 nm is an exciton-like absorption peak which is commonly showed in the 3D bulk film and this peak disappears when higher concentration of PEABr is added. With 80% PEABr concentration in both control and VAC process, the appearance of three pronounced peaks at 400 nm, 435 nm, and 465 nm could be clearly seen in optical spectra, indicating a substantial fraction of 2D nanoplatelets in the 3D structure, which causes reduction of the bulk phase. These results agree well with previous work having PEABr inclusion [6]. The absorption peak at longer wavelength comes from desirable large n-phase or quasi-2D perovskite, and the peaks at shorter wavelengths come from the 2D phases. As VAC leads to more quasi-2D phase, it causes higher absorption coefficient at the longer wavelength. VAC results in better PEABr distribution and incorporation into the 3D in agreement in GIWAXS analysis (Fig. 8).

Figure 2(d) determines band gap values of control and VAC samples from absorbance data. The bandgap energies for both control and VAC samples are 2.639 eV and 2.638 eV, respectively. The values are similar within measurement error as both control and VAC processes utilized the identical perovskite formulae.

Figure 3(a1, b1) show the surface morphologies of control and VAC perovskite films. DMSO, the main solvent used for $CsPbBr_3$ and this work, is known to form intermediate phase [35] with perovskite precursors, disturbing precursor reaction, slowing down crystallization of perovskite materials, and potentially enlarging crystallite size. Conversely, with VAC, more nucleation sites and rapid crystallization occur. Moreover, PEABr addition could also help to achieve smaller grain size by impeding the perovskite crystal growth [6]. However, layered perovskite film is usually composed of the mixture of phases and phase impurities that could cause defect sites and inhomogeneous surface [31]. Figure 3(a1) shows the surface morphology of a control

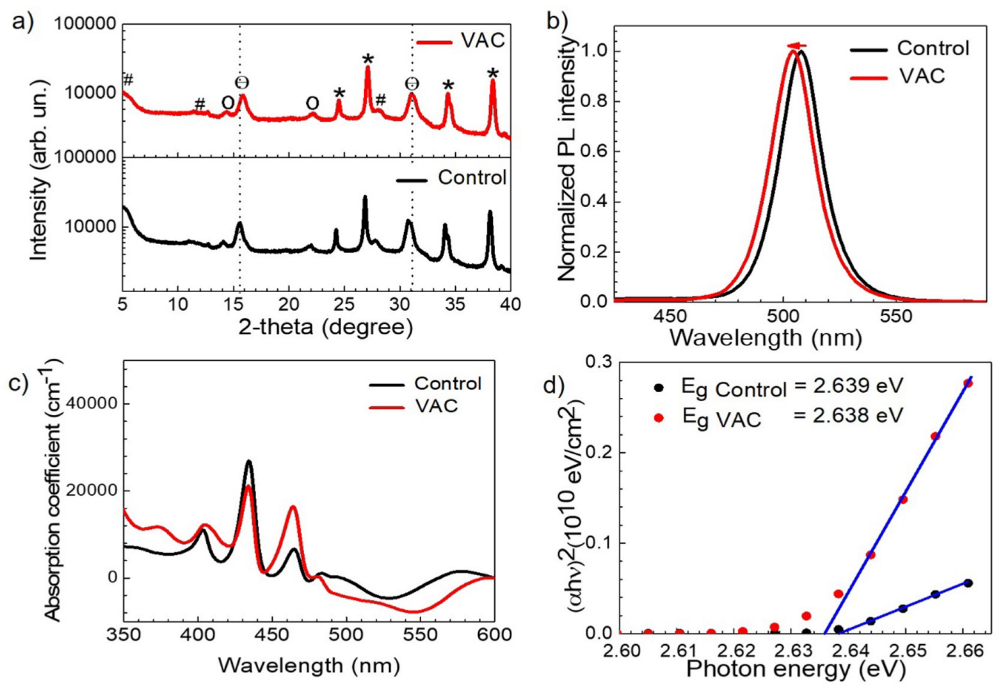

Fig. 2. Identifying crystallinity and optical properties of control and VAC samples a) XRD pattern where (⊖) sign indicates the main peaks of the layered $CsPbBr_3$ perovskite film. (*) sign, (#) sign and (o) indicate FTO peaks, PEABr peaks, and $CsPbBr_3$ peaks, respectively. b) PL intensity, c) Absorbance, and d) Tauc plot for optical band gap estimation.

sample which has small pinholes and some defect spots on the surface which could lead to non-radiative recombination and low emission efficiency. Those defects were from the unwanted phase separation between perovskite and organic phases reported previously [6], consistent with our GIWAXS data. On other hand, the better surface morphology could be observed in VAC sample shown in Fig. 3(b1) as optimized pressure better regulates evaporation rate. Moreover, we estimated grain sizes from SEM images by using ImageJ. Table 1 shows smaller grain sizes for VAC samples. Furthermore, crystallite size is calculated from Scherrer's equation and shown in Table 3 in the appendix. Similar to observation from vacuum treatment for solar cell [22], the thin film became denser and thinner for the same solution concentration as indicated by Fig. 2(c) and Fig. 3(a2, b2). Small grains and thin compact layer can help reduce the diffusion length, yielding strong spatial confinement and increasing the radiative recombination [3,4,26,27].

Table 1. Grain sizes of control and VAC samples.

Condition	Grain size (nm)
Control	57 ± 12
VAC	38 ± 7

Figure 4(a) shows PL intensity of both control and VAC. VAC sample has higher PL intensity, as stronger binding energy due to smaller grains can reduce the dissociation into free electrons. PL lifetime was measured by time correlated single photon counting (TCSPC) to analyze charge dynamics. With tri-exponential fitting, the slow decay time (τ_1) is related to radiative recombination, an important factor for PeLED emission. (τ_2) is the medium decay time caused by

Optical Materials EXPRESS

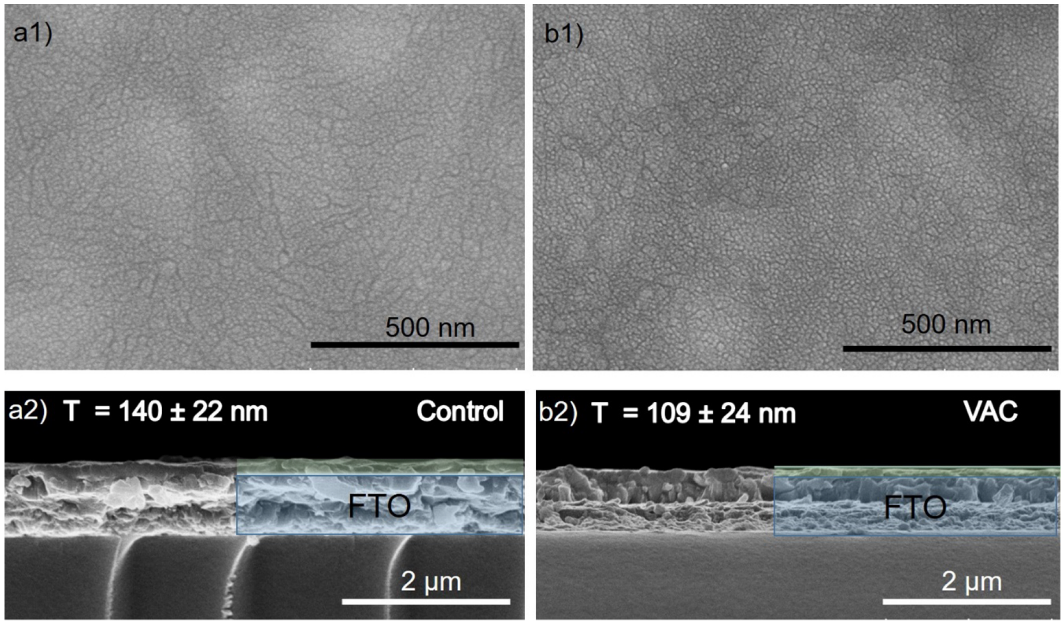

Fig. 3. Comparing morphologies via SEM at high (×1000000) magnifications of control a1) and VAC samples b1), (a2-b2) SEM cross section of both samples to identify film thicknesses.

trap–assisted recombination while (τ_3) is the fastest decay time relating to intrinsic electron–hole recombination [27,29]. When PL lifetime of (τ_1) and (τ_2) are increased, the average PL lifetime is also increased, showing less trap states and non-radiative recombinations [27]. Table 2 shows the average lifetime of both VAC and control samples. Average lifetime of VAC sample is longer than that of control, giving values of 29.00 ns and 13.85 ns, respectively. This increase further signifies that VAC brings about smaller grain and compact formation which lead to more radiative recombination. The absorption band edges of the control and VAC samples appear relatively at the same position as they share the same structures. However, the PL position of VAC sample occurs blue-shift, indicating that it has less trap states [33,34] in both bulk and film surface as in agreement with longer PL-lifetime results in Table 2.

Table 2. Photoluminescence lifetime parameters of control and VAC samples using tri-exponential fitting. The fitting is good with chi-square between 1.16 and 1.41.

Samples	τ_1 (ns)	A_1 (%)	τ_2 (ns)	A_2 (%)	τ_3 (ns)	A_3 (%)	τ_{ave} (ns)
Control	68.60	23.16	12.00	44.54	2.87	32.29	13.85
VAC	78.40	45.18	18.60	44.02	3.71	10.80	29.00

Figure 4(c) shows average photoluminescence quantum efficiencies of VAC sample (63%) compared to that of control (43%). The error bars indicate standard deviation from 6 different samples for each condition. PLQE values further stress the benefit of VAC treatment. To identify stability, PLQEs were measured in 6 different samples for each condition right after preparation and after two months of storage under controlled relative humidity of 60% as shown in Fig. 4(d). Both VAC and control samples have similar resistivity to moisture.

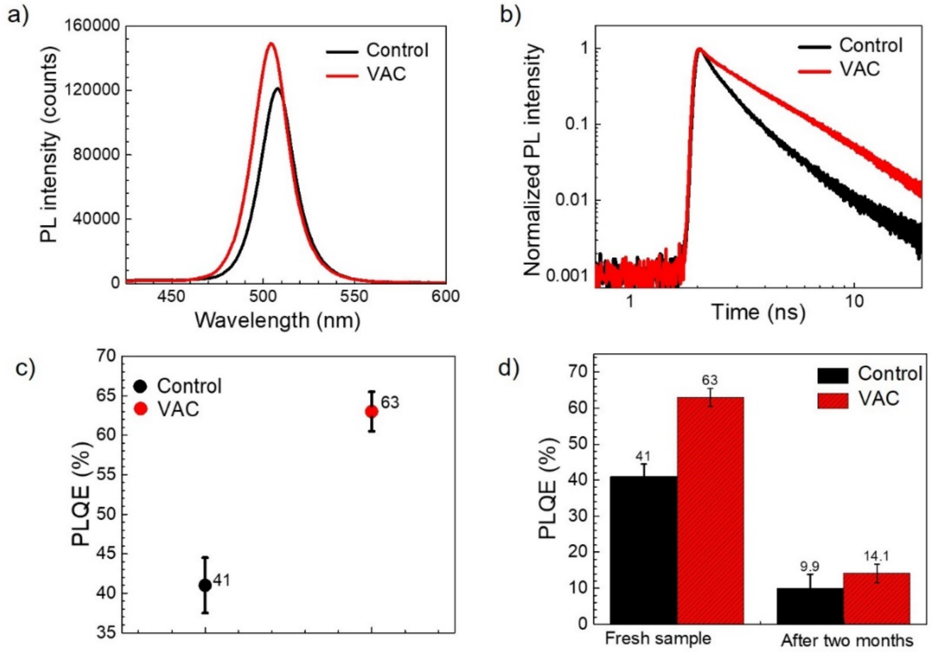

Fig. 4. Performance of perovskite films comparing control and VAC in terms of a) PL intensity, b) time-resolved PL, c) PLQE, and d) Humidity stability by gauging changes in PLQE right after preparation and after 2 months without encapsulation.

4. Conclusions

Vacuum assisted crystallization is a process that allows better crystallization of perovskite film under controlled vacuum environment. With optimized pressure, time duration, and annealing process, VAC regulates solvent evaporation rate, which leads to more nucleation sites, small grain size, improved phase distribution, and denser morphology. These features results in more radiative recombination, higher PL intensity, higher PLQE, and longer PL lifetime with better film stability, highly beneficial for luminescence applications like LED. As VAC is a simple after-deposition technique, VAC could be adapted for various perovskite formula and deposition techniques to improve luminescence properties.

Optical Materials EXPRESS

Appendix

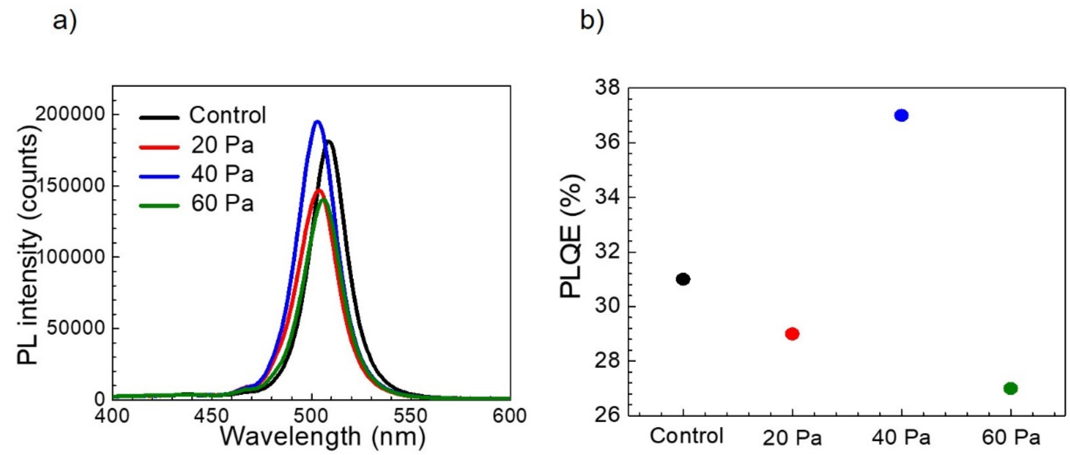

Fig. 5. a) PL and b) PLQE (%) of perovskite films under different vacuum pressures.

Table 3. Crystallite sizes calculated from Scherrer's equation.

Sample	Crystallite size (nm)		Average (nm)
	(100)	(200)	
Control	13.64	11.73	12.68
VAC	12.33	10.18	11.25

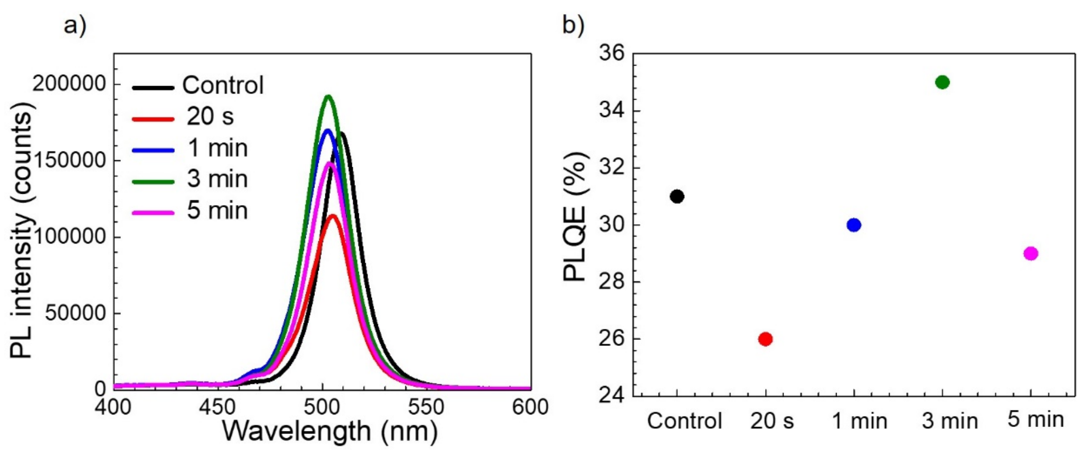

Fig. 6. a) PL and b) PLQE (%) of perovskite films under different holding times inside the vacuum chamber.

Optical Materials EXPRESS

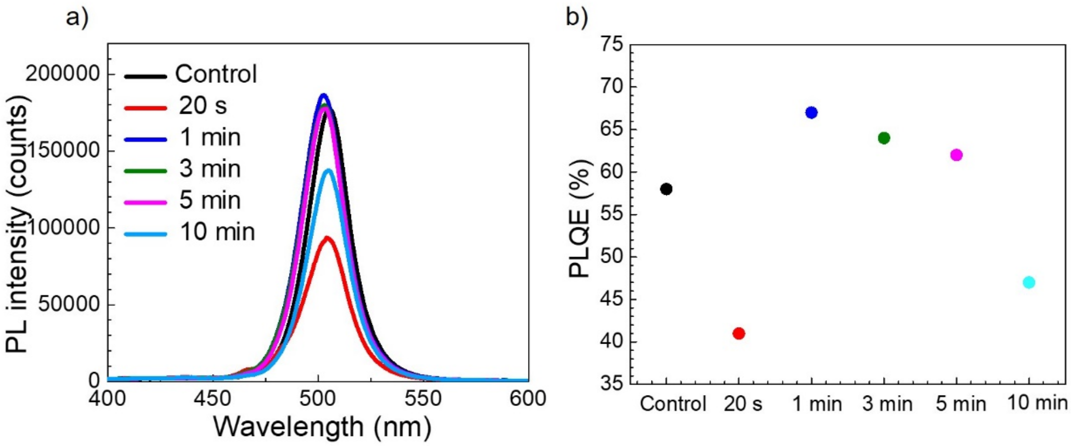

Fig. 7. a) PL and b) PLQE (%) of perovskite films under different annealing times in air. 20 s might not provide enough time, as the films were still wet. For too long annealing times, the perovskite layers became degraded.

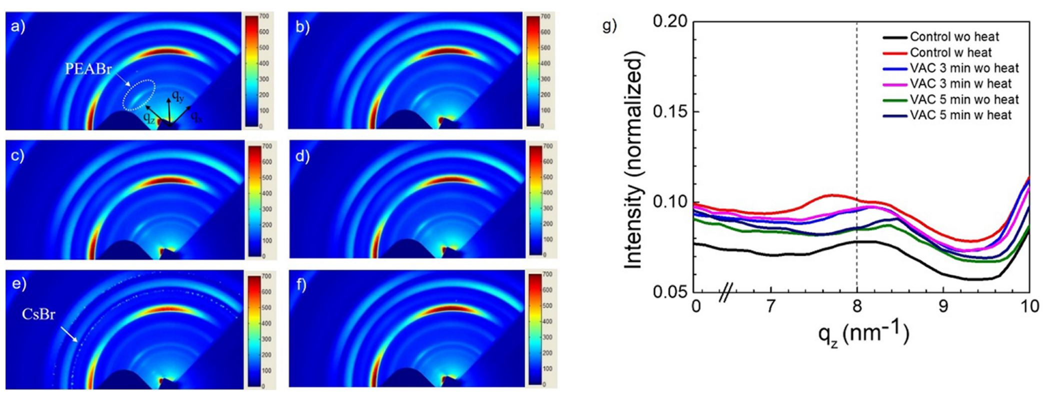

Fig. 8. GIWAXS images for a) Control (without heating), b) Control (with heating), c) 3 mins inside the vacuum chamber and after that without heating, d) 3 mins inside the vacuum chamber and after that with heating, e) 5 mins inside the vacuum chamber and after that without heating, f) 5 mins inside the vacuum chamber and after that with heating, and g) the out-of-plan profile of each condition.

Optical Materials EXPRESS

Funding

Mahidol University (11873); Research Fund for DPST Graduate with First Placement (005/2558); Center of Excellence for Innovation in Chemistry (PERCH-CIC); Faculty of Science, Mahidol University (CIF grant); Thailand Research Fund (MRG6180282); Synchrotron Light Research Institute.

Acknowledgments

We acknowledge Dr. Tanakorn Osotchan and Dr. Toemsak Srikhirin for fruitful discussions. We also would like to acknowledge Ms. Kusuma Pinsuwan for sharing the knowledge about the working mechanism of vacuum controlled setup.

Disclosures

The authors declare no competing interests.

References

1. J. Wang, J. Leng, J. Liu, S. He, Y. Wang, K. Wu, and S. Jin, "Engineered directional charge flow in mixed two-dimensional perovskites enabled by facile cation-exchange," J. Phys. Chem. C **121**(39), 21281–21289 (2017).
2. Y. Kim, H. Cho, J. H. Heo, T. Kim, N. Myoung, C. Lee, S. H. Im, and T. Lee, "Multicolored Organic/Inorganic Hybrid Perovskite Light-Emitting Diodes," Adv. Mater. **27**(7), 1248–1254 (2015).
3. L. Zhang, X. Yang, Q. Jiang, P. Wang, Z. Yin, X. Zhang, H. Tan, Y. M. Yang, M. Wei, B. R. Sutherland, E. H. Sargent, and J. You, "Ultra-bright and highly efficient inorganic based perovskite light-emitting diodes," Nat. Commun. **8**(1), 15640 (2017).
4. P. Kaewurai, J. Ponchai, K. Amratisha, A. Naikaew, K. Z. Swe, K. Pinsuwan, C. Boonthum, S. Sahasithiwat, and P. Kanjanaboos, "Enhancing violet photoluminescence of 2D perovskite thin films via swift cation doping and grain size reduction," Appl. Phys. Express **12**(1), 015506 (2019).
5. A. Naikaew, P. Kumnorkaew, T. Supasai, and S. Suwanna, "Enhancing High Humidity Stability of Quasi-2D Perovskite Thin Films through Mixed Cation Doping and Solvent Engineering," ChemNanoMat **5**(10), 1280–1288 (2019).
6. M. Ban, Y. Zou, J. P. H. Rivett, Y. Yang, T. H. Thomas, Y. Tan, T. Song, X. Gao, D. Credington, F. Deschler, H. Sirringhaus, and B. Sun, "Solution-processed perovskite light emitting diodes with efficiency exceeding 15% through additive-controlled nanostructure tailoring," Nat. Commun. **9**(1), 3892 (2018).
7. N. K. Kumawat, D. Gupta, and D. Kabra, "Recent Advances in Metal Halide-Based Perovskite Light-Emitting Diodes," Energy Technol. **5**(10), 1734–1749 (2017).
8. S. Das, S. Gholipour, and M. Saliba, "Perovskites for Laser and Detector Applications," Energy Environ. Mater. **2**(2), 146–153 (2019).
9. Y. Han, S. Park, C. Kim, M. Lee, and I. Hwang, "Phase control of quasi-2D perovskites and improved light-emitting performance by excess organic cations and nanoparticle intercalation," Nanoscale **11**(8), 3546–3556 (2019).
10. H. Lin, J. Mao, M. Qin, Z. Song, W. Yin, X. Lu, and W. C. H. Choy, "Single-phase alkylammonium cesium lead iodide quasi-2D perovskites for color-tunable and spectrum-stable red LEDs," Nanoscale **11**(36), 16907–16918 (2019).
11. H. Li, Y. Qian, X. Xing, J. Zhu, X. Huang, Q. Jing, W. Zhang, C. Zhang, and Z. Lu, "Enhancing Luminescence and Photostability of CsPbBr3 Nanocrystals via Surface Passivation with Silver Complex," J. Phys. Chem. C **122**(24), 12994–13000 (2018).
12. S. A. Veldhuis, Y. F. Ng, R. Ahmad, A. Bruno, N. F. Jamaludin, B. Damodaran, N. Mathews, and S. G. Mhaisalkar, "Crown Ethers Enable Room-Temperature Synthesis of $CsPbBr_3$ Quantum Dots for Light-Emitting Diodes," ACS Energy Lett. **3**(3), 526–531 (2018).
13. W. Zhang, Y. Jiang, Y. Ding, M. Zheng, S. Wu, X. Lu, X. Gao, Q. Wang, G. Zhou, J. Liu, M. J. Naughton, K. Kempa, and J. Gao, "Solvent-induced textured structure and improved crystallinity for high performance perovskite solar cells," Opt. Mater. Express **7**(7), 2150 (2017).
14. L. C. Chen, Z. L. Tseng, D. W. Lin, Y. S. Lin, and S. H. Chen, "Improved performance of perovskite light-emitting diodes by quantum confinement effect in perovskite nanocrystals," Nanomaterials **8**(7), 459 (2018).
15. W. C. Chang, Y. Y. Cheng, W. C. Yu, Y. C. Yao, C. H. Lee, and H. H. Ko, "Enhancing performance of ZnO dye-sensitized solar cells by incorporation of multiwalled carbon nanotubes," Nanoscale Res. Lett. **7**(1), 166 (2012).
16. J. E. Bishop, J. A. Smith, C. Greenland, V. Kumar, N. Vaenas, O. S. Game, T. J. Routledge, M. Wong-Stringer, C. Rodenburg, and D. G. Lidzey, "High-Efficiency Spray-Coated Perovskite Solar Cells Utilizing Vacuum-Assisted Solution Processing," ACS Appl. Mater. Interfaces **10**(46), 39428–39434 (2018).
17. R. Singh, I. M. Noor, P. K. Singh, B. Bhattacharya, and A. K. Arof, "Synthesis of active absorber layer by dip-coating method for perovskite solar cell," J. Mol. Struct. **1158**, 229–233 (2018).

18. V. Prakasam, D. Tordera, F. Di Giacomo, R. Abbel, A. Langen, G. Gelinck, and H. J. Bolink, "Large area perovskite light-emitting diodes by gas-assisted crystallization," J. Mater. Chem. C **7**(13), 3795–3801 (2019).
19. S. Sánchez, J. Jerónimo-Rendon, M. Saliba, and A. Hagfeldt, "Highly efficient and rapid manufactured perovskite solar cells via Flash InfraRed Annealing," Mater. Today **32**, 1369–7021 (2019).
20. M. M. Byranvand, S. Song, L. Pyeon, G. Kang, G. Y. Lee, and T. Park, "Simple post annealing-free method for fabricating uniform, large grain-sized, and highly crystalline perovskite films," Nano Energy **34**, 181–187 (2017).
21. B. Ding, Y. Li, S. Y. Huang, Q. Q. Chu, C. X. Li, C. J. Li, and G. J. Yang, "Material nucleation/growth competition tuning towards highly reproducible planar perovskite solar cells with efficiency exceeding 20%," J. Mater. Chem. A **5**(15), 6840–6848 (2017).
22. M. Li, H. Yeh, Y. Chiang, U. Jeng, C. Su, H. Shiu, Y. Hsu, N. Kosugi, T. Ohigashi, Y. Chen, P. Shen, P. Chen, and T. Guo, "Highly Efficient 2D/3D Hybrid Perovskite Solar Cells via Low-Pressure Vapor-Assisted Solution Process," Adv. Mater. **30**(30), 1801401 (2018).
23. K. Pinsuwan, C. Boonthum, T. Supasai, S. Sahasithiwat, P. Kumnorkaew, and P. Kanjanaboos, "Solar perovskite thin films with enhanced mechanical, thermal, UV, and moisture stability via vacuum-assisted deposition," J. Mater. Sci. **55**(8), 3484–3494 (2020).
24. J. Chen, J. Xu, L. Xiao, B. Zhang, S. Dai, and J. Yao, "Mixed-Organic-Cation $(FA)_x(MA)_{1-x}PbI_3$ Planar Perovskite Solar Cells with 16.48% Efficiency via a Low-Pressure Vapor-Assisted Solution Process," ACS Appl. Mater. Interfaces **9**(3), 2449–2458 (2017).
25. X. Li, D. Bi, C. Yi, J.-D. Décoppet, J. Luo, S. M. Zakeeruddin, A. Hagfeldt, and M. Grätzel, "A vacuum flash–assisted solution process for high-efficiency large-area perovskite solar cells," Science **353**(6294), 58–62 (2016).
26. H. Cho, S. H. Jeong, M. H. Park, Y. H. Kim, C. Wolf, C. L. Lee, J. H. Heo, A. Sadhanala, N. S. Myoung, S. Yoo, S. H. Im, R. H. Friend, and T. W. Lee, "Overcoming the electroluminescence efficiency limitations of perovskite light-emitting diodes," Science **350**(6265), 1222–1225 (2015).
27. J. Byun, H. Cho, C. Wolf, M. Jang, A. Sadhanala, R. H. Friend, H. Yang, and T. W. Lee, "Efficient Visible Quasi-2D Perovskite Light-Emitting Diodes," Adv. Mater. **28**(34), 7515–7520 (2016).
28. J. Qian, Q. Guo, L. Liu, B. Xu, and W. Tian, "A theoretical study of hybrid lead iodide perovskite homologous semiconductors with 0D, 1D, 2D and 3D structures," J. Mater. Chem. A **5**(32), 16786–16795 (2017).
29. J. Ponchai, P. Kaewurai, C. Boonthum, K. Pinsuwan, T. Supasai, S. Sahasithiwat, and P. Kanjanaboos, "Modifying morphology and defects of low-dimensional, semi-transparent perovskite thin films: Via solvent type," RSC Adv. **9**(21), 12047–12054 (2019).
30. N. K. Noel, A. Abate, S. D. Stranks, E. S. Parrott, V. M. Burlakov, A. Goriely, and H. J. Snaith, "Enhanced photoluminescence and solar cell performance via Lewis base passivation of organic-inorganic lead halide perovskites," ACS Nano **8**(10), 9815–9821 (2014).
31. X. Yang, X. Zhang, J. Deng, Z. Chu, Q. Jiang, J. Meng, P. Wang, L. Zhang, Z. Yin, and J. You, "Efficient green light-emitting diodes based on quasi-two-dimensional composition and phase engineered perovskite with surface passivation," Nat. Commun. **9**(1), 570 (2018).
32. D. Wang, D. Wu, D. Dong, W. Chen, J. Hao, J. Qin, B. Xu, K. Wang, and X. Sun, "Polarized emission from CsPbX3 perovskite quantum dots," Nanoscale **8**(22), 11565–11570 (2016).
33. Q. Han, W. Wu, W. Liu, and Y. Yang, "The peak shift and evolution of upconversion luminescence from CsPbBr3 nanocrystals under femtosecond laser excitation," RSC Adv. **7**(57), 35757–35764 (2017).
34. S. Tanaka, "A New General Synthetical Method of Coumarone. I," Nippon Kagaku Zasshi **72**(3), 307–309 (1951).
35. C. Boonthum, K. Pinsuwan, J. Ponchai, T. Srikhirin, and P. Kanjanaboos, "Reconditioning perovskite films in vapor environments through repeated cation doping," Appl. Phys. Express **11**(6), 065503 (2018).